Quantum Yields of CHDO above 300 nm

Ernst-Peter Röth[1], Luc Vereecken[2]

[1]Institute for Energy and Climate Research IEK-7: Stratosphere, Forschungszentrum Jülich GmbH, 52425 Jülich, Germany

[2]Institute for Energy and Climate Research IEK-8: Troposphere, Forschungszentrum Jülich GmbH, 52425 Jülich, Germany

Corresponding author : Ernst-Peter Röth e.p.roeth@fz-juelich.de

Abstract : *The photolysis of mono-deuterated formaldehyde, CHDO, is a critical process in the deuterium-enrichment of stratospheric hydrogen formed from methane. In this work, a consistent description of the quantum yields of the molecular and radical channels of the CHDO photolysis is deduced from literature data. The fluorescence measurements of Miller and Lee (1978) provided a first data set to deduce the product quantum yields. An alternative analysis is based on the measured quantum yield spectrum for the radical channel of the CD_2O photolysis by McQuigg and Calvert (1969), which is corrected for wavelength dependency and combined with the CH_2O quantum yield spectrum to provide an approximation for CHDO. Both approaches provide consistent results. Finally, the findings of Troe (1984, 2007) enable the specification of the pressure dependence of the quantum yield for CH_2O and CD_2O and, hence, for CHDO. We find that the radical channel does not show a pressure dependence, whereas the molecular channel is dominated by tunneling and quenching processes. Simplified representations are given that are readily implemented in kinetic atmospheric models. As an example of their application, the altitude dependence of the ratio of $J(CHDO \rightarrow HD+CO)$ and $J(CH_2O \rightarrow H_2+CO)$ is provided. Also, the importance of the photolysis of formaldehyde in the atmosphere is presenting the altitudinal dependence of the isotopic fractionation through the yield of the HD channel.*

1. Introduction

Measurements over the last decades showed that molecular hydrogen, H_2, in the stratosphere is enriched in deuterium compared to H_2 in the troposphere (see e.g.: Ehhalt and Volz, 1976; Gerst and Quay, 2001; Rahn et al., 2003; Rice et al., 2003; Röckmann et al., 2003; McCarthy et al., 2004; Rhee et al., 2006). Gerst and Quay (2001) suggested that this enrichment could be due to the differential isotope fractionation in the photo-oxidation of methane. Measurements of the vertical profiles of the isotope content in H_2 and CH_4, available since 2003, allowed the interpretation and modeling of the observed enrichment (see e.g. Pieterse et al., 2011). The methane photo-oxidation consists of various reaction steps, each of which contribute kinetic isotope effects, KIE, that have to be considered (e.g. Feilberg et al., 2005; Mar et al., 2007). The last but critical step in the reaction chain to produce the hydrogen isotope HD from the mono-deuterated isotopologue of formaldehyde, CHDO, is its photolysis.

Compared to CH_2O, the available data for the mono-deuterated isotopologue CHDO are scarce. Only its spectrum was measured (c.f. Mainz Spectral Atlas, Keller-Rudek and Moortgat, 2021). The quantum yields for the molecular and the radical fragmentation branches of the CHDO photolysis, as well as the rate constants for the quenching reactions were not measured at all or with insufficient accuracy. Thus, despite its importance for the atmospheric production of HD, the photolysis of CHDO is still poorly defined; at this time, it is the most uncertain factor in the overall fractionation of formaldehyde. For example, the measured or estimated fractionation factors for the molecular channel range from 1.08 to 1.82 (e.g. Feilberg et al., 2005; Rhee et al., 2006, Mar et al., 2007; Nilsson et al., 2009; Röckmann et al., 2010). Moreover, the measurements by Nilsson et al. (2009) are the only ones considering the pressure dependence of the fractionation factor due to reactions R3, R4, and R7 (see Table 1).

In this work, we aim to provide information for the modeling of CHDO photochemistry for atmospheric conditions, i.e. for a limited domain of temperature and pressure, by deducing the molecular and radical quantum yields Φ^{mol} and Φ^{rad} for CHDO from literature information, based on the scant data available and supplemented by a number of plausible assumptions. We do this based on two approaches: the first is based on the fluorescence measurements of Miller and Lee (1978) and literature data on energy transitions (e.g. Yeung and Moore, 1973; Chuang et al., 1987; Osborn, 2008; Fu et al. 2011). The second approach assumes that the

measurements of McQuigg and Calvert (1969) can be corrected via the comparison of the CH_2O measurement with later experiments (see e.g. the overview by Röth and Ehhalt, 2015). The photochemistry derived thus is then used to assess the altitudinal dependence of the CHDO isotopic fractionation.

2. Photolysis reaction mechanism

Based on the available literature (e.g.: Aràujo et al., 2009; Breuer and Lee, 1971; Chuang et al., 1987; Yamaguchi et al., 1998) we propose a photolytic reaction scheme of CHDO in Table 1, analogous to that of CH_2O (Röth and Ehhalt, 2015). The scheme involves a cascading series of fragmentation channels competing with stepwise quenching by collisional energy loss, starting at the excited singlet state S_1. Reactions via the triplet state of CHDO are not considered here, as they are only accessible at wavelengths below 300 nm (Aràujo et al.,2009), while we concentrate on wavelengths above this limit in this work. Under atmospheric conditions, which are considered here, the system is thermalized.

Table 1 : Reaction scheme of the photolysis of CHDO occurring over the S_1 and S_0 electronic singlet states. $-\Delta\varepsilon 1$, $-\Delta\varepsilon 2$ indicate the collisional energy losses to bath gas M in the respective reactions. This quenching is stepwise but is represented here for energies above/below the threshold for dissociation; the asterix * stands for excitations able to lead to bond breaking, whereas the index # indicates lower energies and lead ultimately to thermalized CHDO.

$$CHDO(S_0) + h\upsilon \rightarrow CHDO^{*}(S_1) \quad \text{(R0)}$$

$$CHDO^{*}(S_1) \rightarrow CHDO^{\#} + h\nu_1 \quad \text{(R1)}$$

$$CHDO^{*}(S_1) \rightarrow CHDO^{*}(S_0) \quad \text{(R2)}$$

$$CHDO^{*}(S_0) \rightarrow H+CDO \,/\, D+CHO \quad \text{(R2a)}$$

$$CHDO^{*}(S_0) \rightarrow CO + HD \quad \text{(R2b)}$$

$$CHDO^{*}(S_0) + M \rightarrow CHDO^{\#}(S_0) + M \quad \text{(R2c)}$$

$$CHDO^{*}(S_1) + M \rightarrow CHDO^{*\text{-}\Delta\varepsilon 1}(S_0) + M \quad \text{(R3)}$$

$$CHDO^{*\text{-}\Delta\varepsilon 1}(S_0) \rightarrow H+CDO \,/\, D+CHO \quad \text{(R3a)}$$

$$CHDO^{*\text{-}\Delta\varepsilon 1}(S_0) \rightarrow CO + HD \quad \text{(R3b)}$$

$$CHDO^{*\text{-}\Delta\varepsilon 1}(S_0) + M \rightarrow CHDO^{\#}(S_0) + M \quad \text{(R3c)}$$

$$CHDO^{*}(S_1) + M \rightarrow CHDO^{*\text{-}\Delta\varepsilon 2}(S_1) + M \quad \text{(R4)}$$

$$CHDO^{*\text{-}\Delta\varepsilon 2}(S_1) \rightarrow CHDO^{\#}(S_0) + h\nu_5 \quad \text{(R5)}$$

$$CHDO^{*-\Delta\varepsilon 2}(S_1) \rightarrow CHDO^{*-\Delta\varepsilon 2}(S_0) \quad (R6)$$

$$CHDO^{*-\Delta\varepsilon 2}(S_0) \rightarrow H+CDO \,/\, D+CHO \quad (R6a)$$

$$CHDO^{*-\Delta\varepsilon 2}(S_0) \rightarrow CO + HD \quad (R6b)$$

$$CHDO^{*-\Delta\varepsilon 2}(S_0) + M \rightarrow CHDO^{\#}(S_0) + M \quad (R6c)$$

$$CHDO^{*-\Delta\varepsilon 2}(S_1) + M \rightarrow \ldots \quad (R7)$$

After excitation of the ground state CHDO(S_0) (R0) by a photon of a given wavelength, the excited reaction product CHDO*(S_1) decays by fluorescence (R1), or transitions to the S_0 ground state surface as an excited CHDO* molecule with either all available energy (R2) or with a variable amount of energy -Δε1 lost by quenching (R3). These excited CHDO*(S_0) and CHDO*$^{-\Delta\varepsilon 1}$(S_0) can in turn be quenched by the bath gas in a cascading series (R2c, R3c, R6c), at each energy level competing with fragmentation to radicals H+CDO/D+CHO (R2a, R3a,R6a) or to molecular products CO+HD (R2b, R3b,R6b), as described for CH_2O by Yeung and Moore, (1973). Alternatively, the excited CHDO*(S_1) can lose an amount of energy by quenching, but remain on the S_1 excited electronic surface (R4). This state can then undergo processes as above, i.e. decay by fluorescence (R5), transition to the S_0 ground state without (R6) or with (R7) energy loss by quenching, where once again it can undergo further quenching (R6c) in competition with fragmentation (R6a, R6b). Overall, this scheme represents a cascading series of quenching steps competing against decomposition and fluorescence. Only the first few steps in the cascade are represented, but more cascading steps are possible at lower internal energies. According to the analysis of the fluorescence measurements by Miller and Lee (1978), these lower-energy reactions are not critical and need not be considered in detail. Here, R7 simply represents the summation of all subsequent cascades, from which negligible channels such as *e.g.* the fluorescence channels are omitted. Schematic energy diagrams for this reaction mechanism were already depicted in the literature (e.g. Fig.3 in Aràujo et al., 2009 and Fig.1 in Chuang et al., 1987), and are not repeated here.

The quantum yield Φ^{rad} represents the combined fragmentation to radicals (R2a, R3a, R6a), while summed fragmentation through the molecular branches (R2b, R3b, R6b) is described by the quantum yield Φ^{mol}. The total photolysis quantum yield Φ^{tot}, i.e. the decay of excited formaldehyde into products other than its ground-state, can be experimentally derived from the observed CO production, where CDO and CHO radical fragments react with O_2 to form

CO and HO_2 / DO_2. The quantum yield of the fluorescence is always less than 1% (Miller and Lee, 1978) and is omitted henceforth.

$$\Phi^{tot} = \Phi^{mol} + \Phi^{rad} \quad \text{(F1)}$$

Obviously, the sum of Φ^{tot} and Φ^{quench}, the summed yield of the quenching reactions (R2c, R3c, R6c), must equal 1 at any wavelength hν.

$$\Phi^{tot} + \Phi^{quench} = 1 \quad \text{(F2)}$$

3. Analysis of fluorescence measurements

From the fluorescence measurements of Miller and Lee (1978) the quantum yields of both the fluorescence and the total non-CHDO products can be derived. The contribution of the second step in the reaction cascade is small at low pressure (see later), so we assume that Table X provided by these authors directly gives the reaction rate constants k_1 and k_2, where k_1 equals the reciprocal lifetime $\tau_{radiation}$ listed and $1/k_2$ is the non-radiative lifetime. Similarly, the constants k_5 and k_6 are determined by the lifetimes of the next lower vibrational level.

The reaction constants k_3, k_4, and k_7 can be deduced from the pressure dependence of the CHDO fluorescence quantum yield in the Table II of Miller and Lee (1978). In the present paper only the quantum yields at pressures above 1 Torr are considered, where the Ar bathgas used is assumed to have similar collisional properties as air (Hirschfelder et al.,1954). For each wavelength the pressure dependence of the data is fitted by a Simplex algorithm according to Nelder and Mead (1965) by formula F3 for the fluorescence quantum yield Φ_F.

$$\Phi_F(M) = \frac{k_1}{\alpha} + \frac{k_4[M]}{\alpha}.\frac{k_5}{\beta} \quad \text{(F3)}$$

with $\alpha = k_1 + k_2 + k_3[M] + k_4[M]$ and $\beta = k_5 + k_6 + k_7[M]$.For consistency we only used the 2^i4^j transitions, only.

The corresponding reaction constants are listed in Table 2. With this data set the experimental fluorescence measurements are well fitted as shown in Figure 1 where, to improve the clarity of the fit, only the pressure dependent part θ(M) of equation F3 is plotted vs pressure:

$$\theta(M) = \frac{k_1}{\phi_F(M)} - (k_1 + k_2) \quad \text{(F4)}$$

Table 2 : Results of the least square fit of the quantum yields of CHDO (Miller and Lee (1978). k_1, k_2 and k_5, k_6 are literature data (Miller and Lee, 1978), k_3, k_4, and k_7 are deduced from these data.

Wavelength [nm]	k_1 [$10^5 s^{-1}$]	k_2 [$10^8 s^{-1}$]	k_3 [$10^{-11} cm^3 s^{-1}$]	k_4 [$10^{-11} cm^3 s^{-1}$]	k_5 [$10^5 s^{-1}$]	k_6 [$10^8 s^{-1}$]	k_7 [$10^{-12} cm^3 s^{-1}$]
314.0	3.03	1.79	29.7	4.59	2.78	0.50	0.57
318.3	2.50	1.32	15.4	3.48	2.50	0.40	1.15
325.7	2.78	0.50	10.9	1.77	3.57	0.22	1.79
330.8	2.50	0.40	4.81	1.05	2.44	0.13	1.35
338.6	3.57	0.22	4.89	0.84	3.45	0.07	0.77
344.4	2.44	0.13	5.95	2.78	2.40*	0.06*	1.39
352.9	3.45	0.07	2.38	0.76	4.00*	0.03*	1.24

* estimated by extrapolation of the other values

The energy transferred in reaction R2 is either quenched to form a stable molecule $CHDO^{\#}(S_0)$ or used to drive fragmentation to molecular (CO + HD) or radical products (H+CDO / D+CHO). Hence, the reactions R2a and R2b form part of the product-forming channel. Analogously, the secondary reactions of the pressure dependent reactions R3 and R4 lead to products via the reactions R3a and R3b, respective R6a and R6b. With this, the total product quantum yield of the photolysis of CHDO is the sum of the individual product quantum yields across all channels k, where the index k=2, 3, 6 stands for the non-radiative reactions R2, R3, and R6.

The individual product quantum yield can be approximated by

$$\Phi_k^{tot} = \frac{1}{1+a \cdot exp\left(\frac{\varepsilon_k - \varepsilon_0}{b}\right) \cdot \frac{[M]}{[M_0]}} \qquad \text{(F5)}$$

analog to the publication by Röth and Ehhalt (2015) on CH_2O.

In equation F5, ε_2 is the excitation energy of the photolysis reaction. The energies ε_3 and ε_6 are related to ε_2 by the approximated energy transfer in a collision, respective by the averaged width of the band intervals, given by $\varepsilon_3 = \varepsilon_2$ -0.0124 eV (Troe, 2007) and $\varepsilon_6 = \varepsilon_2$ -0.13 eV (Miller and Lee, 1978). The pivot wavelength $1/\varepsilon_0$ is 348.6 nm, as published in Nilsson et al. (2014) from quantum chemical calculations of the barriers to dissociation of H-CHO, H-CDO, D-CHO, and D-CDO.

The total quantum yield of the products (molecules plus radicals) can be deduced from the rate constants of Table 2 and the measurements of Nilsson et al. (2010, 2014), who

investigated the pressure dependence of the kinetic isotope effect KIE of the photolysis frequencies of CH_2O and CHDO.

$$KIE = \frac{j_{CH2O}}{j_{CHDO}} \qquad \text{with} \quad j = \int \Phi^{tot}_{CH2O/CHDO}\, \sigma F d\lambda \tag{F6}$$

As the quantum yield of CH_2O is known from the literature (see e.g. Röth and Ehhalt, 2015) Φ^{tot}_{CHDO} remains the only unknown factor in formula F6. With the actinic flux density F of the lamp used by Nilsson et al. (2014) and the absorption spectra σ_x of CH_2O and CHDO from Gratien et al. (2007) the ratio KIE can be calculated with optimized values for *a* and *b* in eq. F5. Comparing the results of the simulation with the measured data by Nilsson et al. (2010, 2014) the constants *a* and *b* can be determined via a least square fit. Figure 2 presents the result with optimized values *a*=2.94 and *b*=6.5×10^{-5} nm^{-1} together with the measurements. The data at 1000 hPa is included in the fit as its mean value to accommodate the large variation of the data.

The total product quantum yield, deduced from the reaction scheme R0 to R7 is

$$\Phi^{tot} = \frac{k_2}{\alpha} \cdot \Phi_2^{tot} + \frac{k_3[M]}{\alpha} \cdot \Phi_3^{tot} + \frac{k_4[M]}{\alpha} \cdot \frac{k_6}{\beta} \cdot \Phi_6^{tot} \tag{F7}$$

with α and β as defined in formula F3, and Φ_k^{tot}, the sub-product yield, according to formula F5. The measured wavelength dependence of Φ^{tot} at 1000 hPa pressure is depicted in Figure 3, where the total quantum yield is calculated with the rate constants from Table 2. The pressure dependence of the three terms of Φ^{tot} is illustrated in Figure 4.

To obtain a continuous and smooth wavelength dependence, the rate constants k_1 through k_7 can be represented by an approximation function

$$k = A \exp (B (\lambda\text{-}300nm)) \tag{F8}$$

The values for the parameters A and B are obtained from a least square fit to the data in Table 2 and listed in Table 3. Where-ever the value of B was less than 0.001 it was set to 0, and A then corresponds directly to the mean of the respective rate constant. The wavelength dependence of Φ^{tot} at 1000 hPa with these functions is presented by the solid line in Figure 3. The comparison to the experimental data by Miller and Lee (1978) suggests a variance of the data of around 15%.

Table 3: Parameters of the rate constants according to equation F8, B in nm^{-1} and A in s^{-1}, respective in cm^3 s^{-1}, derived from least square fits.

	k_1	**k_2**	**k_3**	**k_4**	**k_5**	**k_6**	**k_7**

A	2.90×10^{5}	6.10×10^{8}	7.70×10^{-10}	1.30×10^{-10}	3.00×10^{5}	1.50×10^{8}	1.2×10^{-12}
B	0	0.086	0.069	0.071	0	0.075	0

For CHDO the only quantitative indication for the quantum yield of the radical channel in the literature are measurements of the kinetic isotope effect KIE (Feilberg et al., 2007, Rhee et al., 2008, Röckmann et al., 2010, and Nilsson et al., 2014). Folowing eq. F5, simulating these KIE-measurements requires three parameters for the individual radical quantum yield Φ_k^{rad} expressed in eq. F9: the maximum value Φ^{max} of the wavelength dependence, its curvature *b*, and the pivot wavelength λ_0. The parameter a is set to 1, as for the radical quantum yield no pressure dependence is assumed, cancelling the [M]/[M_0] factor.

$$\Phi_k^{rad} = \frac{\Phi^{max}}{1+a exp\left(\frac{\varepsilon_k-\varepsilon_0}{b}\right)} \qquad \text{(F9)}$$

Analog to the analysis for CH_2O (Röth and Ehhalt, 2015), where the curvatures of the wavelength dependence of Φ^{tot} and Φ^{rad} are similar, *b* can be set to 6.5×10^{-5} nm^{-1} for the radical quantum yield of CHDO. The maximum Φ^{max} was varied in the interval [0.70 / 0.78] around the corresponding value for CH_2O, but the resulting scattering is very small (see shaded area in Fig. 5). Consequently, parameter Φ^{max} is set to 0.74, matching the value also used for CH_2O (Ehhalt and Röth, 2015).

With these parameters the KIE of 1.63 as measured by Röckmann et al. (2010) was fitted with the actinic flux density given by Röckmann et al. and the optical spectra by Gratien et al. (2007). The best fit gave a pivot wavelength λ_0 of 327 nm. This value lies in the middle of the bond energies of 362.63 kJ/mol for C-H and 369.6 kJ/mol for C-D, calculated by Chuang et al. (1987). With the constants Φ^{max} = 0.74, *a*=1, *b* = 6.5 10^{-5} nm^{-1} and $1/\varepsilon_0$ = 327.1 nm the quantum yield function Φ^{rad} of the radical channel of CHDO is analog to F7:

$$\Phi^{rad} = \frac{k_2}{\alpha}\cdot\Phi_2^{rad} + \frac{k_3[M]}{\alpha}\cdot\Phi_3^{rad} + \frac{k_4[M]}{\alpha}\frac{k_6}{\beta}\cdot\Phi_6^{rad} \qquad \text{(F10)}$$

where the radical quantum yields of the individual channels is given by function F9 and with α and β as defined in F3. Figure 5 depicts the wavelength dependence of the total quantum yield together with that for the radicals. At atmospheric pressures, as considered in this paper, the contributions of the individual quenching processes are insignificant with respect to the overall radical quantum yield.

To provide a more handy tool for atmospheric modeling, we introduce an exponential function (F11), with only one term and three parameters for the total and the radical quantum

yields of CHDO, similar to those deduced by Ehhalt and Röth (2015) for CH_2O, as a proxy for the three-term functions F7 and F10:

$$\Phi = \frac{a}{1+exp\left(\frac{-\left(\frac{1}{\lambda}-\frac{1}{\lambda_0}\right)}{b}\right)\frac{[M]}{[M_0]}} \qquad \text{(F11)}$$

The corresponding parameters for the total quantum yield of CHDO are a=1.0, b=7.7×10^{-5} s^{-1}, and λ_0=336.2 nm. For the radical channel the factor [M]/[M_0] is set to 1, as the photolysis leading to the radicals is nearly pressure independent. The respective parameters are a=0.74, b=7.7×10^{-5} s^{-1}, and λ_0=325.0 nm. Both approximation curves are depicted in Figure 5, and Figure 6 shows the pressure dependent comparison with the measured data by Miller and Lee (1978).

4. Analysis of the CHDO photo-decomposition

Our second approach to estimate the quantum yields for the photolysis of CHDO is based on the experiments of McQuigg and Calvert (1969) who measured the photo-decomposition of CH_2O, CHDO, and CD_2O. Unfortunately, the authors only presented the quantum yields for the two radical reaction channels of CH_2O and CD_2O. They further assumed that the total quantum yield equals 1, independent of wavelength. It appears, however, that these data have a bias which becomes evident when the data for CH_2O are compared to more recent measurements.

In Figure 7 the dependence on the wavelength of Φ^{rad} of CH_2O by McQuigg and Calvert (1969) is depicted together with a curve for CH_2O, averaged over measured data from the paper by Röth and Ehhalt (2015). The latter evaluation showed no pressure dependence, but indicated a weak temperature effect which is neglected here. The curve is represented by the following function:

$$\Phi_{CH2O}^{rad} = \frac{0.74}{1+exp\left(\frac{-\left(\frac{1}{\lambda}-\frac{1}{327.4}\right)}{5.4\times10^{-5}}\right)} - \frac{0.40}{1+exp\left(\frac{\frac{1}{\lambda}-\frac{1}{279.0}}{5.2\times10^{-5}}\right)} \qquad \text{(F12)}$$

Equation F12 exhibits a maximum in Φ^{rad} around 310 nm, independent of the small temperature shift, whereas the earlier values of McQuigg and Calvert exhibit a monotonic decay with increasing wavelength above 280 nm, which points to a bias in the latter. The second summand in F12 is less than 1% at wavelengths above 300 nm and, hence, can be

omitted in the present paper. Figure 7 also includes the data of McQuigg and Calvert (1969) for CD_2O which show a quite similar wavelength dependency as the data for CH_2O.

Our first assumption is that the bias in the experiments of McQuigg and Calvert extends equally to both isotopologues (CD_2O and CH_2O), and that, therefore, the ratio R of their quantum yields is correct. This ratio is displayed in Figure 8 and shows a mostly monotonic decrease with increasing wavelength. In this context, it is interesting to note that the ratio of the rate constants for the decomposition of excited CH_2O^* and CD_2O^* into the respective radical channels, as calculated by Troe (1984) from theory, result in a curve with a monotonic decrease with increasing wavelength similar to that of the quantum yield ratio (see Figure 8). Using ratio R together with the fit function F12 for Φ_{CH2O}^{rad} allows to estimate Φ_{CD2O}^{rad} for the radical channel of CD_2O, as shown in Figure 8.

To calculate Φ_{CHDO}^{rad} we need one further assumption. Our hypothesis is suggested by the results of Feilberg et al. (2004), who found that the KIE of the reactions of CHDO with OH, Cl and Br are arithmetic means of the KIE of the reactions of CH_2O and CD_2O with those radicals. This in turn implies that the C-H bond strengths are similar in the isotopologues, and the same is true for the C-D bond strength. We, therefore, assume that Φ_{CHDO}^{rad} can be calculated from the average of Φ_{CH2O}^{rad} and Φ_{CD2O}^{rad} at each wavelength:

$$\Phi_{CHDO}^{rad}(\lambda) = \left(\Phi_{CH2O}^{rad}(\lambda) + \Phi_{CD2O}^{rad}(\lambda)\right)/2 \qquad \text{(F13)}$$

The resulting radical quantum yields are compared in Figure 9. Φ_{CHDO}^{rad} does not depend on pressure since neither Φ_{CH2O}^{rad} nor Φ_{CD2O}^{rad} are pressure dependent. The respective maxima in Φ^{rad}, on the other hand, decrease from 0.72 over 0.70 to 0.65 for increasing deuteration. Moreover, there is a blue shift of 5 nm, resp. 10 nm in the decreasing part of the quantum yield spectra of CHDO and CD_2O, i.e. at wavelengths above 315 nm. These blue shifts have the same tendency but do not quite match the measured threshold energies of 362.3 kJ/mol, 368.4 kJ/mol, and 370.6 kJ/mol for CH_2O, CHDO, and CD_2O, respectively (Chuang et al.,1987), which correspond to the wavelengths 330.9 nm, 325.5 nm, and 323.5 nm.

The one-term fit function for the radical channel of CHDO is:

$$\Phi_{CHDO}^{rad} = \frac{0.72}{1+exp\left(\frac{-\left(\frac{1}{\lambda}-\frac{1}{323.0}\right)}{7.7\times10^{-5}}\right)} \qquad \text{(F14)}$$

and is also show in Figure 9. In Figure 10 the result of the interpretation of the measured photo-decomposition of CHDO by McQuigg and Calvert (1969) is compared to the radical

quantum yield deduced from the fluorescence measurements of Miller and Lee (1978). Both estimations lead to a wavelength dependence of Φ_{CHDO}^{rad} which lie in each others uncertainty range. This is a strong hint that the deduced results are robust and represent the true quantum yield of the radical channel of the photolysis of CHDO.

5. The isotope fractionation during the photolysis of formaldehyde

The photolysis frequency J_i of the isotopologues CH_2O and CHDO is given by the integration of quantum yield Φ, absorption cross section σ, and spectral actinic photon flux density $F_\lambda(\lambda)$ over the λ wavelength domain:

$$J_i = \int \Phi_{i,j}(\lambda) \cdot \sigma_i(\lambda) \cdot F_\lambda(\lambda)\, d\lambda \quad \text{(F15)}$$

where the quantum yield $\Phi_{i,j}(\lambda)$ depends on the product channel j, either molecular or radical, of isotopologue i, and the absorption cross section $\sigma_i(\lambda)$ is specific to the isotopologues i. For our calculations the absorption spectra of CH_2O and CHDO from Gratien et al. (2007) were applied. We used these values instead of the JPL-recommendation (Burkholder, 2020) for consistency with the calculations in section 2 and 3. The solar spectral actinic flux density F_λ was calculated from a quasi-spherical 1-D radiation transfer model (Röth, 2002); the $\Phi(\lambda)$ are those from section 2. An example of the terms $\Phi^{mol}(\lambda)$, $\sigma(\lambda)$, $F_\lambda(\lambda)$ for the molecular channel of CHDO is given in Figure 11 for the pressure and temperature at an altitude of 20 km. The product of these terms, integrated over 5 nm intervals for better visibility, is also displayed to demonstrate the spectrally resolved contributions to the photolysis frequency of the molecular channel of CHDO.

The kinetic isotope effect for the molecular channel is given by

$$KIE_{mol} = \frac{J_{CH2O}^{mol}}{J_{CHDO}^{mol}} \quad \text{(F16)}$$

and correspondingly for the radical channel

$$KIE_{rad} = \frac{J_{CH2O}^{rad}}{J_{CHDO}^{rad}} \quad \text{(F17)}$$

For a quick overview the dependence of KIE_{rad} and KIE_{mol} on altitude for globally averaged conditions (equinox, 30°N) are depicted in Figures 12a and 12b. KIE_{mol} decreases monotonically with decreasing pressure from 1.59 at 1000 hPa to 1.06 at 1 hPa. The radical channel in contrast shows hardly any pressure dependency as the rate of this reaction is not influenced by the quenching process. The marginal variation of the kinetic isotope effect with

altitude is caused by the altitudinal increase of the photon flux and its differing contribution to the photolysis frequency integrals of CH_2O and CHDO.

To examine whether the quantum yield functions for CHDO deduced above are applicable for modeling purposes, additional sensitivity studies were carried out, varying the main features of the quantum yield functions. With respect to the fractionation factor, only the variations of those parameters are relevant which alter the relation of the entire photolysis frequency integrals (eq. F15) of the molecular and the radical channels. In Figures 12a and 12b we additionally show the variances of the photolysis frequencies as well as of the fractionation factors. The shaded area is produced by varying one parameter of the CHDO quantum yield as indicated below. The photolysis frequency of CH_2O remained unchanged.

The sensitivity of the molecular branch of the photolysis frequency of CHDO to the preexponential factor of the quantum yield function is roughly 10 % throughout the atmosphere if this value is varied by 10%. All other parameters do not alter the integral equation F15 significantly and produce only variances less than 1 % when changed by 10%. It can thus be concluded that the estimated equation parameters are good representations of the actual values. At higher altitudes (<10 hPa) Φ_{CHDO}^{mol} and Φ_{CH2O}^{mol} are close to unity in the wavelength regime 330 nm to 360 nm (see e.g. Fig. 6). So, the photolysis frequency in the stratosphere does not change much if the parameters of the respective functions are varied. Therefore, the variance of the fractionation factor does not much decrease above 30 km altitude. Here, measurements at tropospheric pressures could be much more informative as becomes evident from Figure 12.

The photolysis frequency of the radical channel of CHDO is only sensitive to the maximum of the quantum yield and to the threshold wavelength 323 nm. Shifting the latter value by ± 3 nm produces changes of about 20 % in the troposphere, decreasing to 10 % at 50 km altitude as shown in Figure 12. This variation of the threshold produces an error bar of the fractionation factor of the same magnitude.

6. Discussion

Due to consecutive reactions only the molecular channel contributes to the HD production. Up to now there had been a handicap in the interpretation of stratospheric measurements of the concentration of deuterated hydrogen HD due to the lack of exact knowledge of the photolysis frequencies of deuterated formaldehyde, resulting in an uncertainty on the fractionation factor. There have been a number of experimental approaches to deduce the fractionation factor, where e.g. Feilberg et al. (2005) measured a value of 1.82±0.07 for α_{mol}, while Röckmann et al. (2010) found a value of 1.63 ± 0.03 for that ratio. In their modeling paper, Mar et al. (2007) varied the fractionation factor between 1.2 and 1.5 for stratospheric conditions.

In all these studies the pressure dependence of the photolysis frequencies could not be investigated. An interesting experiment by Nilsson et al. (2009) addressed this problem. Unfortunately, the spectral radiance of the light source used did not resemble the sun light well enough, and their findings could not be transferred to the real atmosphere without information on the quantum yield of CHDO.

Beside its pressure dependence the variation of the photolytic fractionation factors can also be caused by different actinic fluxes at the times and sites of the experiments. The actinic flux in the numerator and denominator of the fractionation factor in equations F16 and F17 do not cancel out, and, therefore, the factor is depending on the local insolation conditions. Calculations of the solar zenith angle (SZA) dependency with the complex radiation transfer model ART (Röth, 2002) result in values from 1.47 at overhead sun to 1.95 at SZA=83° for clear sky and free horizon at ground level. This zenith angle dependency is less expressed at 20 km altitude and disappears at 50 km, as depicted in Figure 13. This effect may explain the differences in the measurements of the fractionation factors. To check the variance with the solar zenith angle the measured fractionation factor KIE_m (eq. F16) is compared to model calculations. The factor 1.63 ±0.03 (Röckmann et al., 2010) was derived from experimental studies in the atmospheric simulation chamber SAPHIR between 60° and 70° SZA (Röckmann et al., 2010). The absorption cross sections by Gratien et al. (2007) and the quantum yields derived above together with the radiation spectra result in a fractionation factor of 1.54 for 60° SZA and 1.70 for 70° SZA are in good agreement with the measured value.

Conclusions

The current work derives a framework and set of equations for describing the CHDO photolysis, based on two different approaches building on the available literature data, finding a consistent result across all data sets. It could be shown that the most influential parameters of the rates of photolysis of CHDO are the absolute value and the threshold of the quantum yield of the radical channel. Simplified parametrized equations (F11 and F14) that are readily implemented in kinetic models are provided for these quantities. Measurements around 300 nm and 325 nm could help to further reduce the uncertainty on the fractionation factor. Additional measurements of the pressure dependence of the total quantum yield, i.e. the quenching rate of excited $CHDO^*$, would be valuable to further test the assumptions made in this paper.

Competing interests

The authors declare they have no competing interests

Acknowledgments

The authors thank Dr. B. Bohn and Dr. D. Tarraborrelli for their useful comments and suggestions to improve the clarity and readability of the paper.

References

Araùjo, M., Lasome, B., Magalhaes, A. L., Worth, G. A., Bearperk, M. J., and Robb, M. A.
The molecular dissociation of formaldehyde at medium photoexcitation energies: A quantum chemistry and direct quantum dynamics study
J. Chem. Phys. 131, 144301-1 – 144301-8, 2009

Breuer, G. M., and Lee, E. K. C.
Fluorescence decay times of Cyclic Ketones, Acetone, and Butanal in the gas phase
J. Phys. Chem. 75, 989 – 990, 1971

Burkholder, J. B., Sander, S. P., Abbatt, J. P. D., Barker, J. R., Cappa, C., Crous, D., Dipple, T. S., Huie, R. E., Kolb, C. E., Kurylo, M. J., Orkin, V. L., Percival, C. J., Wilmouth, D. M., and Wine, P. H.
Chemical kinetics and photochemical data for use in atmospheric studies
JPL-Publication 19-5, Pasadena, 2020

Chuang, M-C., Foltz, M. F., and Moore, C. B.
T_1 barrier height, S_1-T_1 intersystem crossing rate, and S_0 radical dissociation threshold for H_2CO, D_2CO, and HDCO
J. Chem. Phys. 87, 3855 – 3864. 1987

Ehhalt, D. H., Volz, A.
Coupling of the CH_4 with the H_2 and CO cycle : isotopic evidence
In : Symposium on Microbiol. Production and Utilization of Gases (H_2, CH_4, and CO)
(eds.: Schlegel, H. G., Gottschalk, G., Pfenning, N.), Akad. Wiss. Göttingen, Germany, 1976

Feilberg, K. L., Johnson, M. S., Nielsen, C. J.
Relative Reaction Rates of HCHO, HCDO, DCDO, $H^{13}CHO$, and $HCH^{18}O$ with OH, Cl, Br, and NO_3 Radicals.
J. Phys. Chem. A 108, 7393 – 7398, 2004

Feilberg, K. L., D'Anna, B., Johnson, M. S., Nielsen, C. J.
Relative Tropospheric Photolysis Rates of HCHO, $H^{13}CHO$, $HCH^{18}O$, and DCDO Measured at the European Photoreactor Facility
J. Phys. Chem. 109A, 8314 – 8319, 2005

Feilberg, K. L., Johnson, M. S., Bacak, A., Röckmann, T., Nielsen, C. J.
Relative Tropospheric Photolysis Rates of HCHO and HCDO Measured at the European Photoreactor Facility
J. Phys. Chem. 111A, 9034 – 9046, 2007

Fu, B., B.Shepler, B. C., and Bowman, J. M.
Three-State Trajectory Surface Hopping Studies of the photosissociation dynamics of formaldehyde on ab initio potential energy surfaces
J. Am. Chem. Soc. 133, 7957 – 7968, 2011

Gerst, S., Quay, P.
Deuterium component of the global molecular hydrogen cycle
J. Geophys. Res., 106, 5021 – 5031, 2001

Gratien, A., Nilsson, E., Doussin, J-F., Johnson, M. S., Nielsen, C. J., Stenstrom, Y., and Picquet-Varrault, B.
UV and IR Absorption Cross-sections of HCHO, HCDO, and DCDO
J. Phys. Chem., 111A, 11506 – 11513, 2007

Hirschfelder, J. O., Curtiss, C. F., and Bird, R. B.
Molecular Theory of Gases and Liquids
Wiley, London, 1249pp., 1954

Keller-Rudek, H., G. Moortgat, G. K., Sander, R., and Sörensen, R.
MPI-Mainz UV-VIS Spectral Atlas of Gaseous Molecules
http://www.atmosphere.mpg.de/enid/2295
Last access 01.06.2022

Mar, K. A., McCarthy, M. C., Connell, P., K. Boering, K. A.
Modelling the photochemical origins of the extreme deuterium enrichment in stratospheric H_2
J. Geophys. Res. 112, D19302, doi: 10.1029/2006JD007403, 2007

McCarthy, M. C., K. Boering, A., Rahn, T., J. Eiler, J. M., Rice, A. L., Tyler, S. C., Schauffler, S., Atlas, E., D. Johnson, D. G.
The hydrogen isotopic composition of water vapor entering the stratosphere inferred from high-precision measurements of δD-CH_4 and δD-H_2
J. Geophys. Res. 109, D07304, doi:10.1029/2003JD004003, 2004

McQuigg, R. D., Calvert, J. G.
The Photodecomposition of CH_2O, CD_2O, CHDO, and CH_2O-CD_2O Mixtures at Xenon Flash Lamp Intensities
J. Am. Chem. Soc. 91, 1590 – 1599, 1969

Miller, R. G. and Lee, E. K. C.
Single vibronic level photochemistry of formaldehydes in the A $^1A_2$ state: Radiative and nonradiative processes in H_2CO, HDCO, and D_2CO
J. Chem. Phys. 68, 4448 – 4464, 1978

Nelder, J. A. , and Mead, R.
A simplex method for function minimization
Computer Journal, 7, 308 -313, 1965

Nilsson, E. J. K., Bache-Andreassen, L., Johnston, M. S., and Nielsen, C. J.
Relative Tropospheric Photolysis Rates of Acetaldehyde and Formaldehyde Isotopologues Measured at the European Photoreactor Facility
J. Phys. Chem. 113A, 3498 – 3504, 2009

Nilsson, E. J. K., Andersen, V. F., Skov, H., and Johnson, M. S.
Pressure dependence of the deuterium isotope effect in the photolysis of formaldehyde by ultraviolet light
Atmos. Chem. Phys. 10, 3455 – 3463, 2010

Nilsson, E. J. K., Schmidt, J. A., and Johnson, M. S.
Pressure dependent isotopic fractionation in the photolysis of formaldehyde-d2
Atmos. Chem. Phys. 14, 551 – 558. 2014

Osborn, D.L.
Exploring multiple reaction paths to a single product channel
Adv. Chem. Phys. 138, 213 – 265, 2008

Pieterse, G., Krol, M. C., Batenburg, A. M., Steele, L. P., Krummel, P. B., Langenfels, R. I., and Röckmann, T.
Global modelling of H_2 mixing ratios and isotopic compositions with the TM5 model
Atmos. Chem: Phys., 11, 7001 – 7026, 2011

Rahn, T., Eiler, J. M., Boering, K. A., Wennberg, P. O., McCarthy, M. C., Tyler, S., Schauffler,. S., Donelly, S., Arlas, E.
Extreme deuterium enrichment in stratospheric hydrogen and the global atmospheric budget of H_2
Nature 424, 918 – 921, 2003

Rhee, T. S., Brenninkmeijer, C. A. M., Braß, M., Brühl, C.
Isotopic composition of H_2 from CH_4 oxidation in the stratosphere and the troposphere
J. Geophys. Res. 111, D23303, doi:10.1029/2005JD00670, 2006

Rhee, T. S., Brenninkmeijer, C. A. M., and Röckmann, T.
Hydrogen isotope fractionation in the photolysis of formaldehyde
Atmos. Chem. Phys. 8, 1353 – 1366, 2008

Röckmann, T., Rhee, T. S., Engel, A.
Heavy hydrogen in the stratosphere
Atmos. Chem. Phys. 3, 2015 -2023, 2003

Röckmann, T., Walter, S., Bohn, B., Wegener, R., Spahn, H., Brauers, T., Tillmann, R., Schlosser, E., Koppmann, R., and Rohrer, F.
Isotope effect in the formation of H_2 from H_2CO studied at the atmospheric Simulation chamber SAPHIR
Atmos. Chem. Phys. 10, 5343 – 5357, 2010

Röth, E.-P.
Description of the Anisotropic Radiation Transfer Model ART to Determine Photodissociation Coefficients
Ber. Forschungszentrum Jülich, Jül-3960, 2002

Röth, E.-P. and Ehhalt, D. H.
A simple formulation of the CH_2O photolysis quantum yields
Atmos. Chem. Phys. 15, 7195 – 7202, 2015

Troe, J.
Specific rate constants k(E,J) for the unimolecular dissociations of H_2CO and D_2CO
J. Phys. Chem., 88, 4375 – 4380, 1984

Troe, J.
Analysis of quantum yields for the photolysis of formaldehyde at > 310 nm
J. Phys. Chem. A 111, 3868 – 3874, 2007

Yamaguchi, Y., Wesolowski, S., Van Huis, T. J., and Schaefer III, H. F.
The unimolecular dissociation of H_2O on the lowest triplet potential-energy surface
J. Chem. Phys. 108, 5281 – 5288, 1998

Yeung, E.S. and Moore, C. B.
Photochemistry of single vibronic levels of formaldehyde
J. Chem. Phys. 58, 3988 – 3998, 1973

Figures

Fig01 : Comparison of the fluorescence quantum yield measured by Miller and Lee (1978) (full dots) with the fitted function Φ_F (M) (see Eq. F3) for different wavelengths in nm as indicated. To emphasize the quality of the fit, we depict only the pressure dependent part θ(M) as defined in Eq. F4

Fig02 : The pressure dependence of the kinetic isotope effect KIE (i.e. the ratio of the CH_2O/CHDO photolysis frequencies, see Eq. F6) is compared to the measured data of Nilsson et al., 2010 (blue squares), and to Feilberg et al., 2007, Rhee et al., 2008, and Röckmann et al., 2010 (red squares, 'others'). The solid curve at 1000 hPa is included to accommodate the variation of the data.

Fig03: The total product quantum yields Φ^{tot} derived from the measured rate constants of Miller and Lee (1978) at 1000 hPa through Eq. F7 (full circles) is well reproduced by the continuous Φ^{tot} function obtained after fitting the rate coefficients to function Eq. F8 (solid curve).

Fig04: Wavelength dependence of the contributions of the three terms for Φ_2^{tot} , Φ_3^{tot} and Φ_6^{tot} of equation F7 to the total quantum yield Φ^{tot} of the CHDO photolysis at 10 hPa (a) and 1030 hPa (b).

Fig05: The total quantum yields Φ^{tot} of the photolysis of CHDO and that of the radical channel, Φ^{rad}, calculated with the three-term functions Eq. F7 and F10 (black curves). The blue shaded area indicates the variation of parameter a within the interval [0.70 / 0.78]. The red curves, derived using the one-term approximation (eq. F11), and the black curves fall within the variance of each other.

Fig06: Comparison of the one-termfit function F11 (open circles on the solid line) with the measured data (Miller and Lee, 1978) of the total photolytic quantum yields Φ^{tot} (full circles) at 1, 10, 200, and 1000 hPa.

Fig07: The original data of McQuigg and Calvert (1969) for CH_2O (full red squares) and CD_2O (open squares) for the photolytic quantum yields of the radical channel are compared to the averaged function for CH_2O by Röth and Ehhalt (2015).

Fig08: The ratio Φ_{CD2O}/Φ_{CH2O} of the McQuigg and Calvert (1969) data shown in Fig.7 and the corrected radical quantum yield of CD_2O, Φ_{CD2O}^{rad} (black squares). The ratio of the respective reaction constants (triangles) derived theoretically by Troe (1984) shows the same tendency as the quantum yield ratio.

Fig09: Wavelength dependency of the quantum yields Φ^{rad} for the radical channel of the three isotopologues of formaldehyde. The curves for CH_2O (Röth and Ehhalt, 2015) and that for CD_2O (corrected data of McQuigg and Calvert, 1969) are used to calculate the quantum yield of CHDO (black dots) by their mean values. Φ_{CHDO}^{rad} is then fitted by the one-term function Eq. F14 (black line).

Fig10: The CHDO quantum yield Φ_{CHDO}^{rad}fit function deduced from the fluorescence measurements (blue line, Eq. F11) of Miller and Lee (1978), and that from the interpretation of the photo-decomposition (red line, Eq. F14) measurements of McQuigg and Calvert (1969). These lie within the uncertainty range of each other. Also depicted is the function for the total quantum yield Φ^{tot} (Eq. F11)

Fig11 : The photolysis rate is the combination of the actinic photon flux, the absorption cross section and the quantum yield. Depicted are the contributions to the molecular channel of the photolysis rate of CHDO, J_{CHDO}^{mol}, at 20 km altitude and integrated over 5 nm wavelength: the actinic photon flux $F_\lambda(\lambda)$, the absorption cross section $\sigma(\lambda)$ (Gratien et al., 2007), and the quantum yield for the molecular channel $\Phi^{mol}(\lambda)$. The photolysis rate, the photon flux and the cross sectionare multiplied by 2.5×10^5 sec, 2.5×10^{-15} photons^{-1} nm sec, and 1.5×10^{19} cm^{-1}, respectively, to achieve comparability.

Fig12 : The altitudinal dependence of the photolysis frequencies J_{mol} of the molecular channels (a) of CH_2O and CHDO is important for the atmospheric production of HD. For comparison the radical channels (b) are also depicted. The dependence on altitude of the kinetic isotope effect, $KIE = J_{CH2O}/J_{CHDO}$, is more pronounced for the molecular channel than the radical channel. The shaded area indicates the variance upon changing (a) the quantum yield Φ^{mol} by 10% and (b) the radical threshold wavelength by 3 nm.

Fig13 : At 50 km altitude the solar zenith angle dependency of the photolysis frequency ratio of the molecular channel is nearly constant. In contrast, at 0 km the ratio increases significantly for solar zenith angles above 30 degrees.

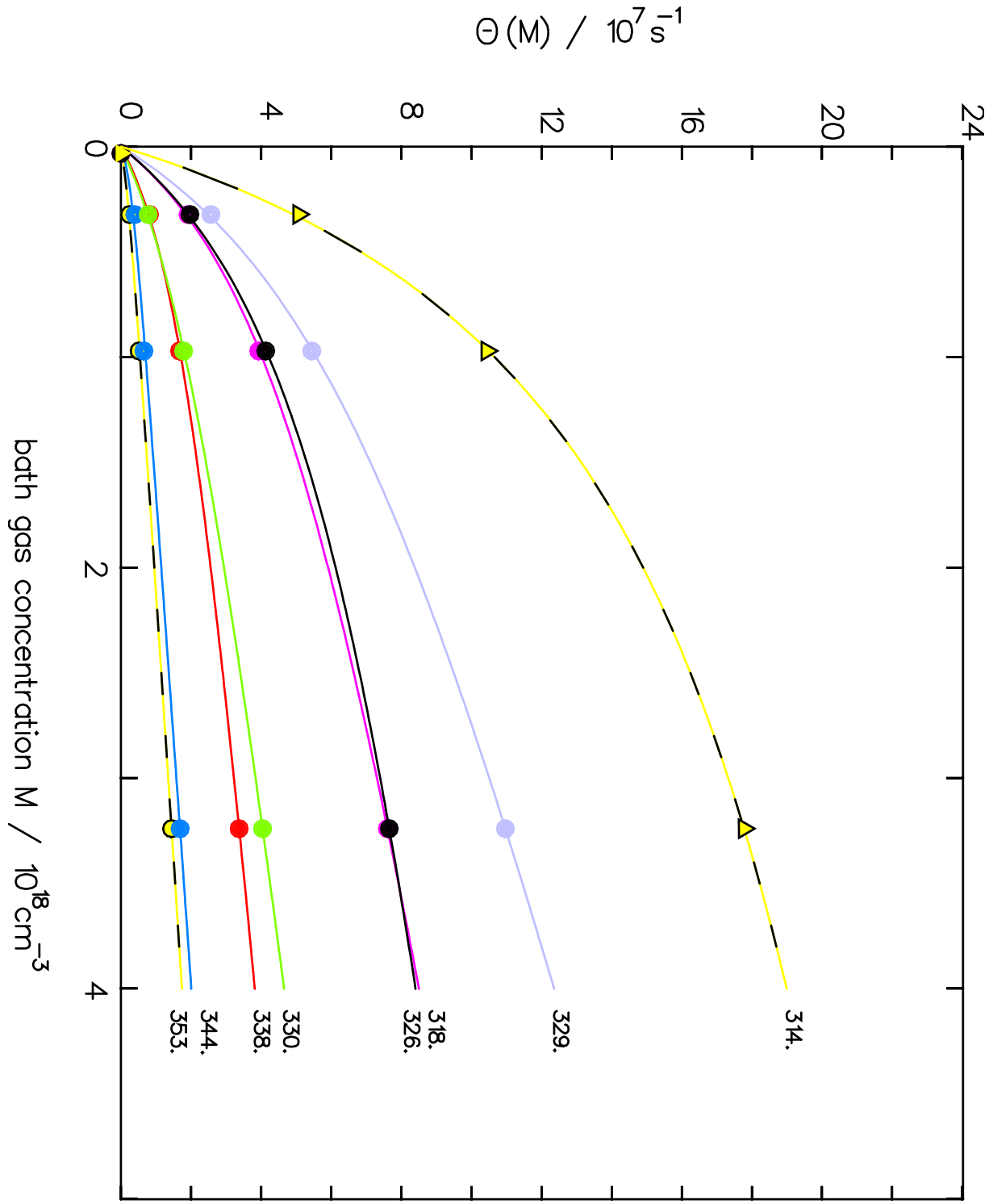

642
643
644
645
646
647

Fig. 1

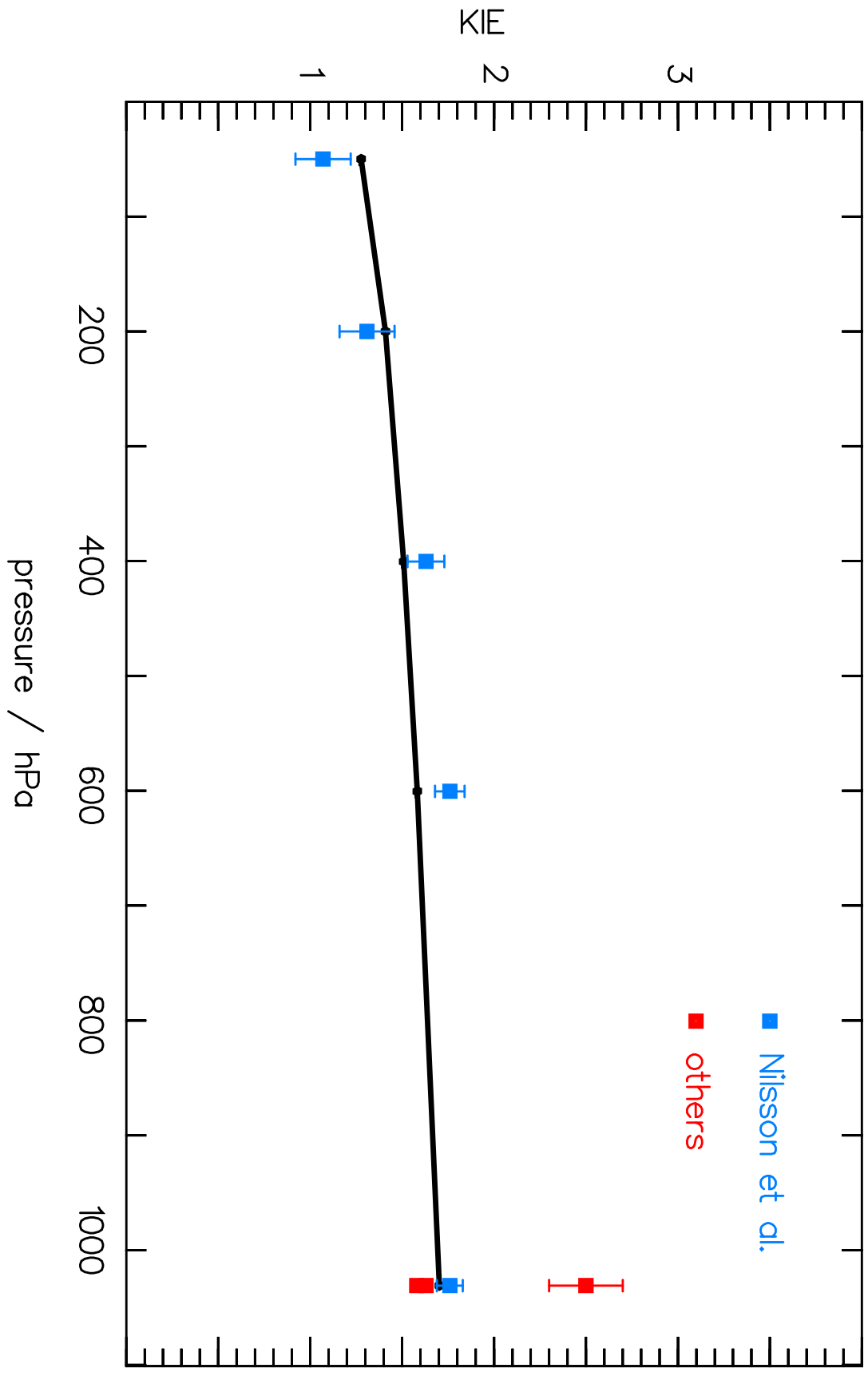
KIE
1
2
3
pressure / hPa
200
400
600
800
1000
Nilsson et al.
others

Fig. 2

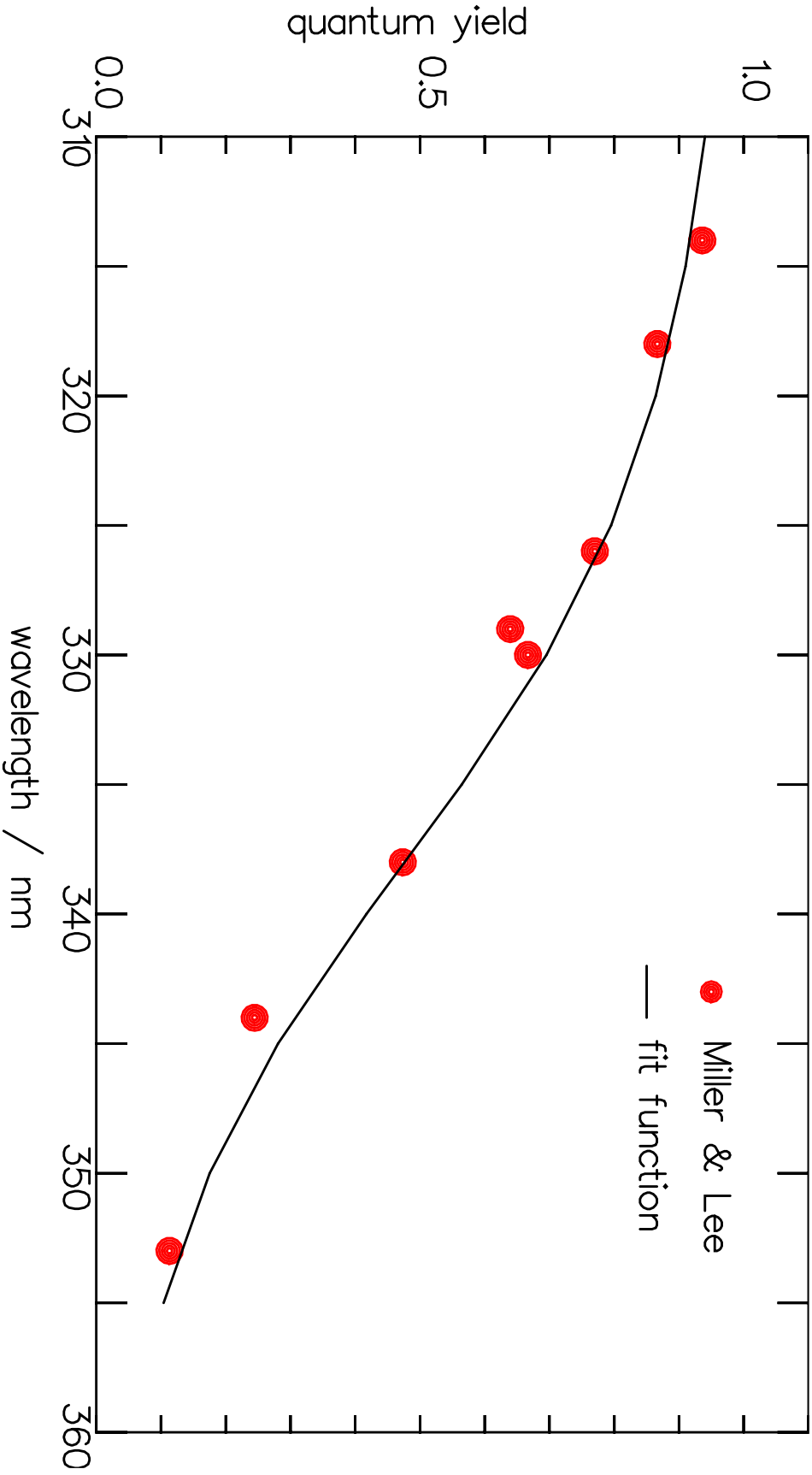
quantum yield
0.0
0.5
1.0
310
320
330
340
350
360
wavelength / nm
Miller & Lee
fit function

Fig. 3

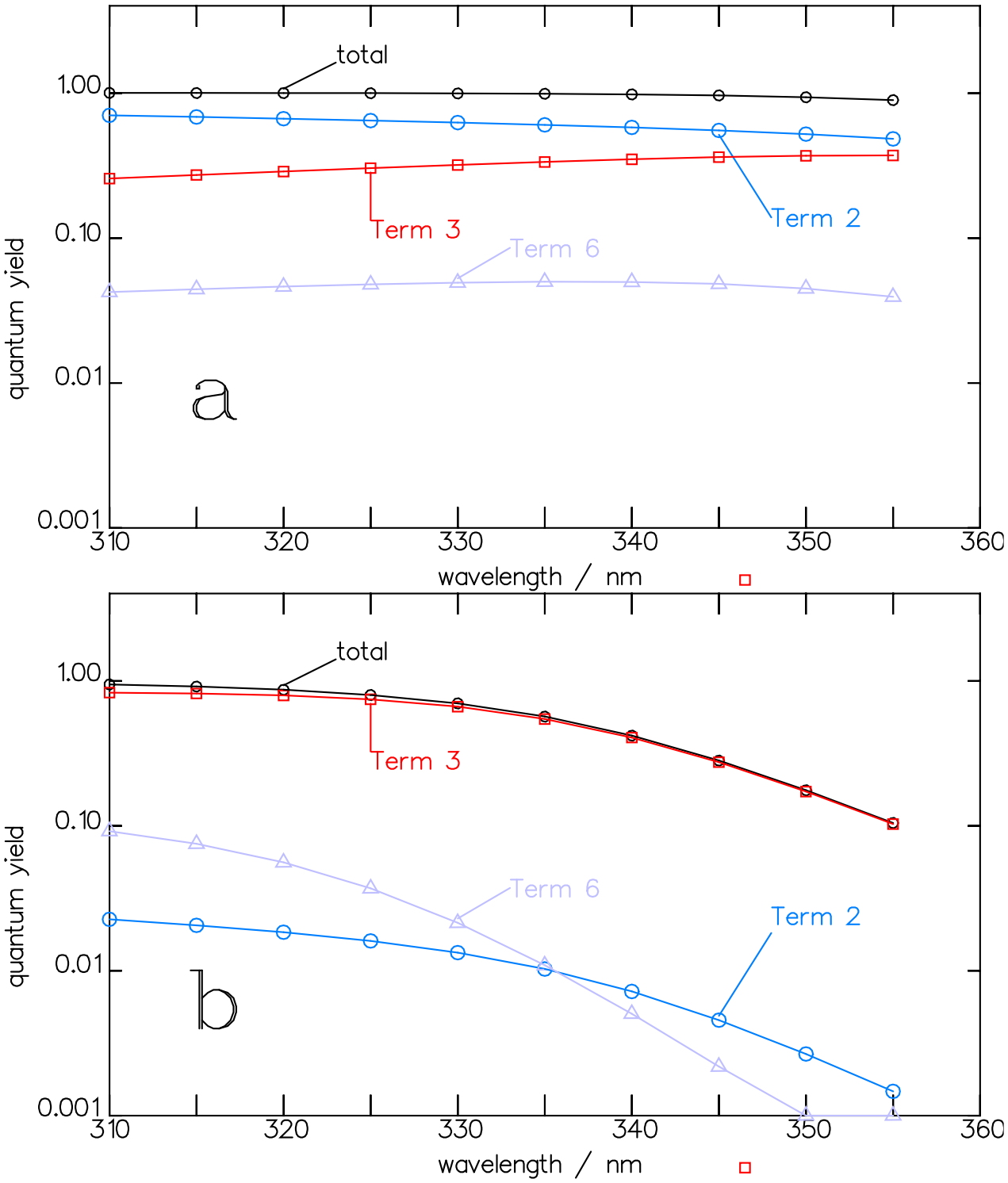
total
Term 3
Term 2
Term 6
quantum yield
1.00
0.10
0.01
0.001
a
310
320
330
340
350
360
wavelength / nm
total
Term 3
Term 6
Term 2
quantum yield
1.00
0.10
0.01
0.001
b
310
320
330
340
350
360
wavelength / nm

Fig. 4

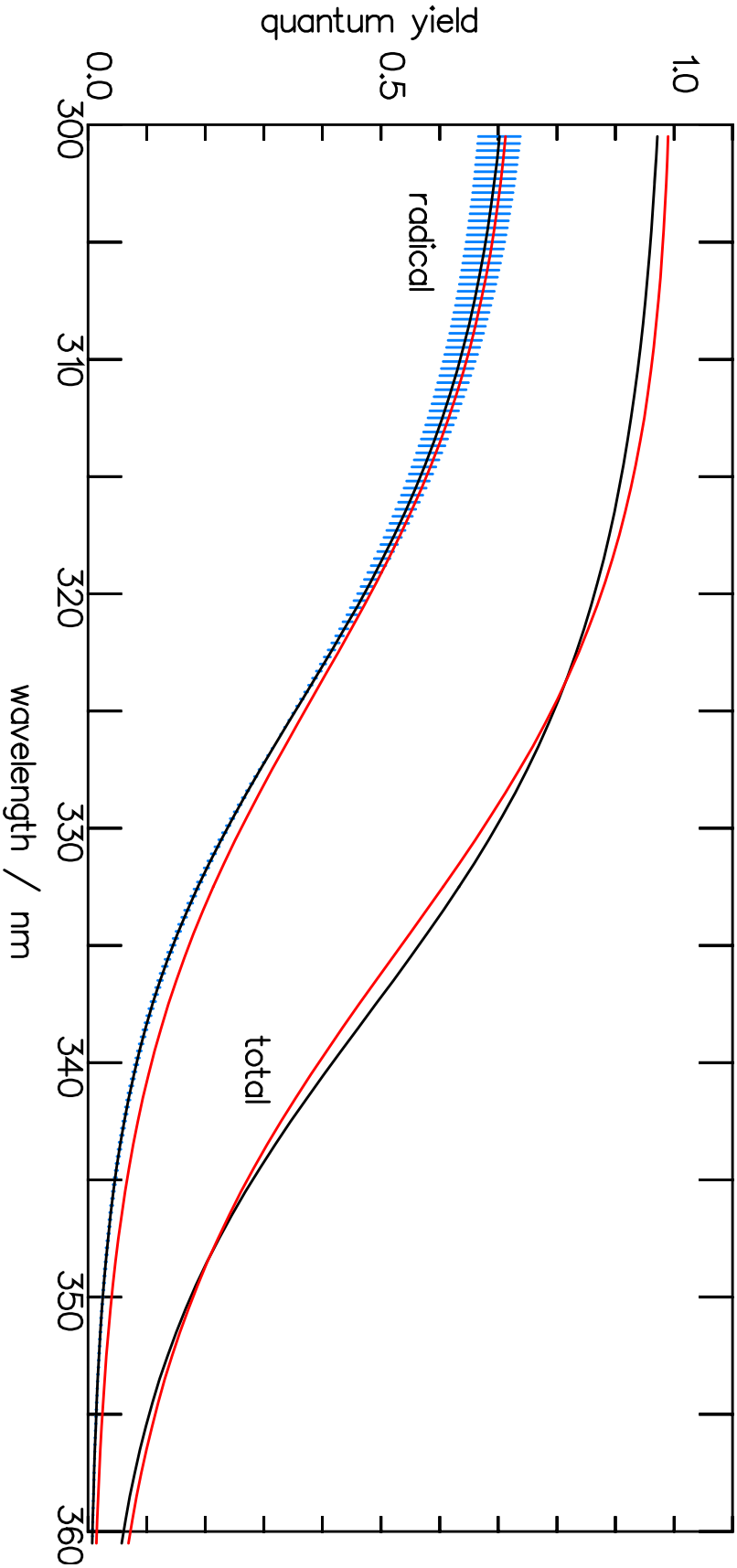
quantum yield
0.0
0.5
1.0
300
310
320
330
340
350
360
wavelength / nm
radical
total

Fig. 5

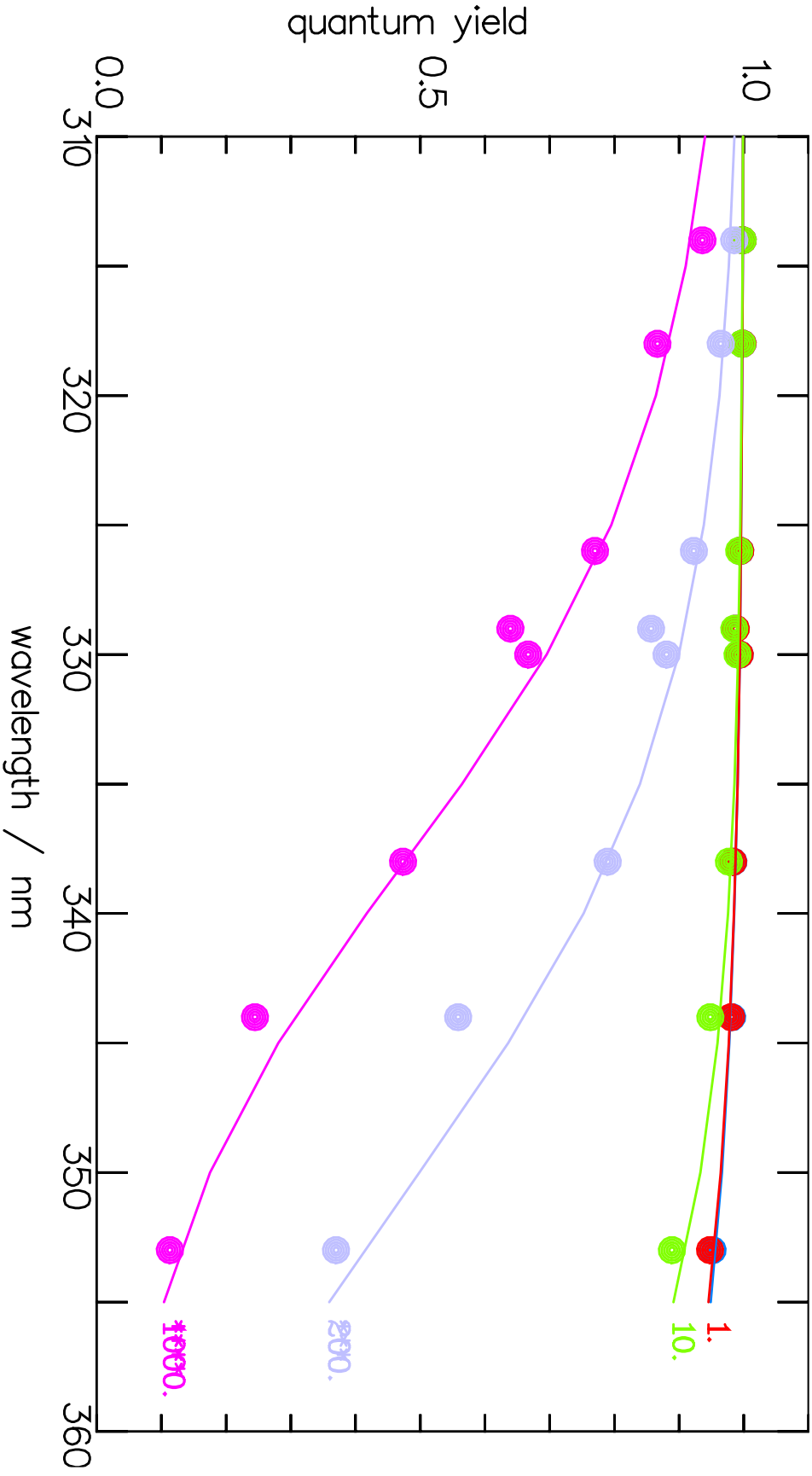
quantum yield
0.0
0.5
1.0
310
320
330
340
350
360
wavelength / nm
1000.
200.
10.
1.

Fig. 6

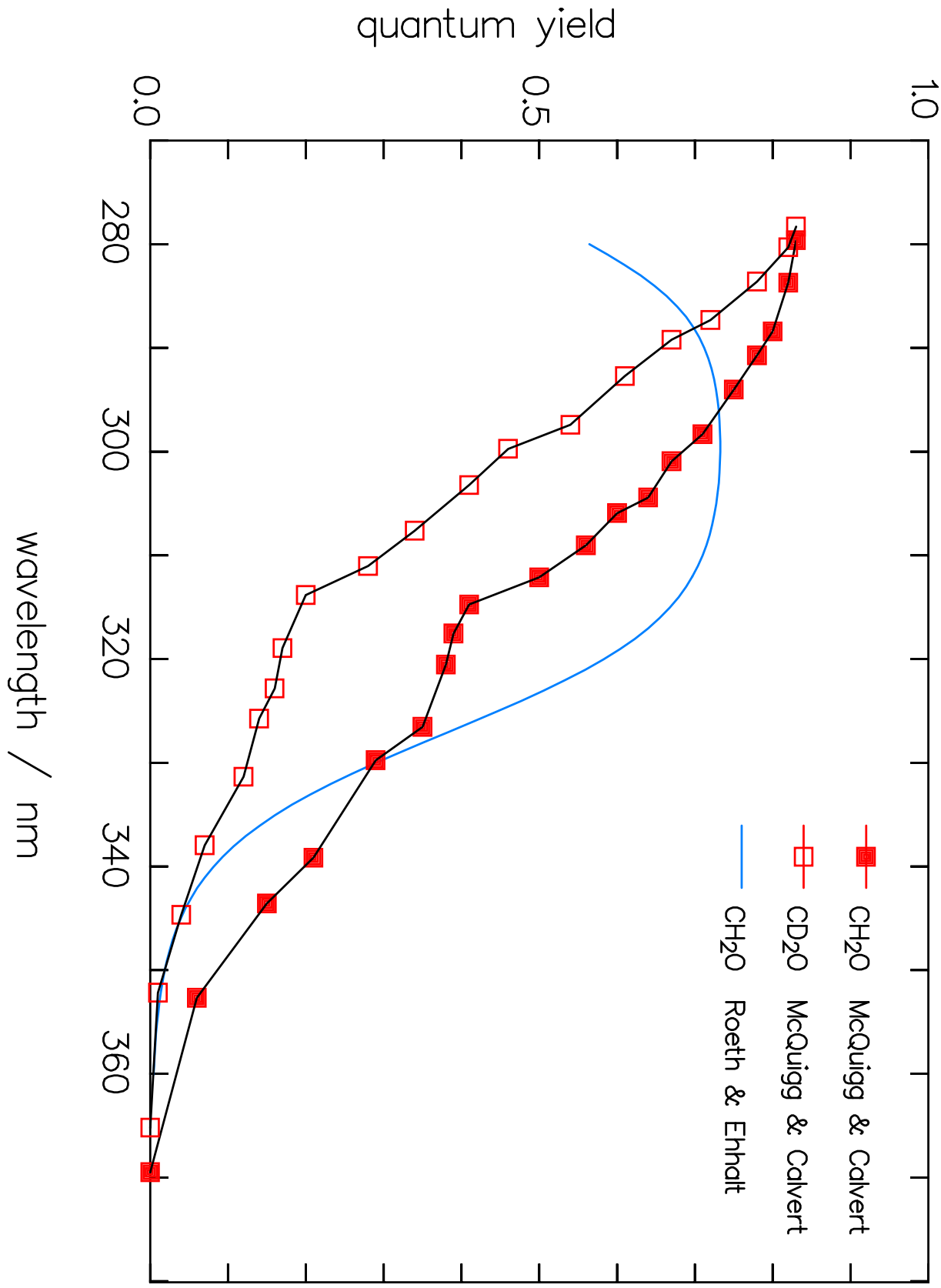
quantum yield
0.0
0.5
1.0
280
300
320
340
360
wavelength / nm
CH2O McQuigg & Calvert
CD2O McQuigg & Calvert
CH2O Roeth & Ehhalt

Fig 7

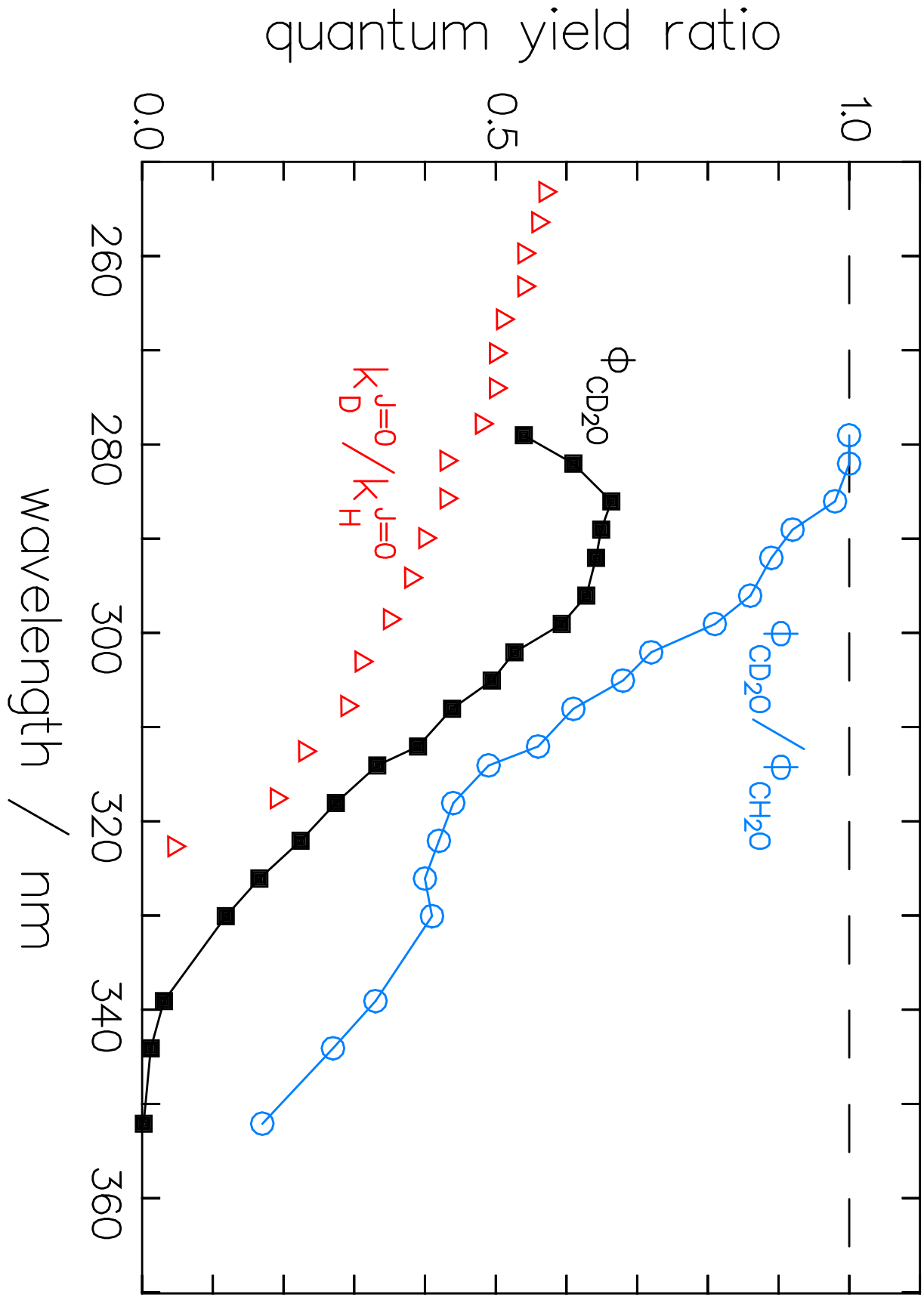

673
674
675
676

Fig. 8

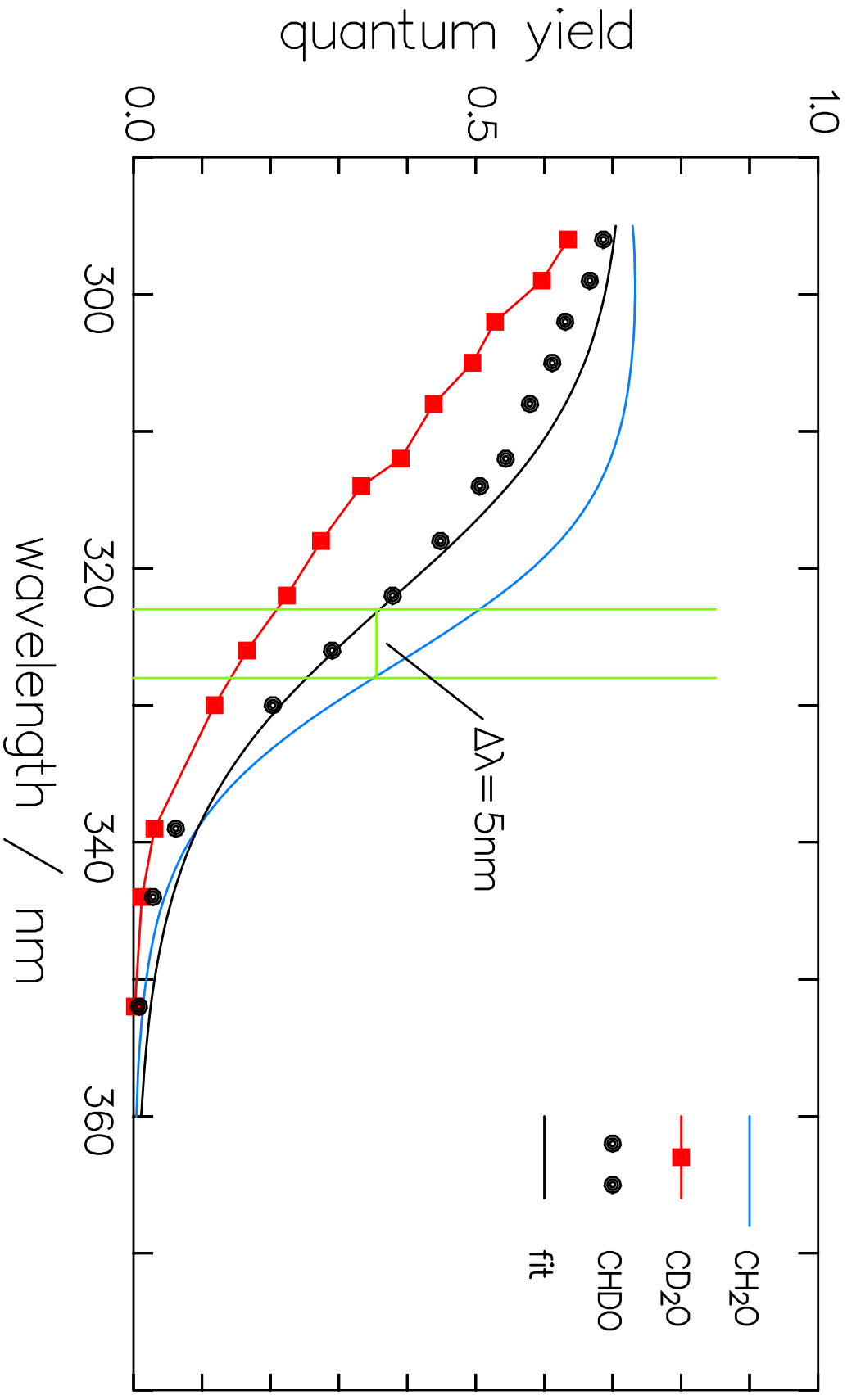
quantum yield
0.0
0.5
1.0
300
320
340
360
wavelength / nm
Δλ= 5nm
fit
CHDO
CD2O
CH2O

Fig. 9

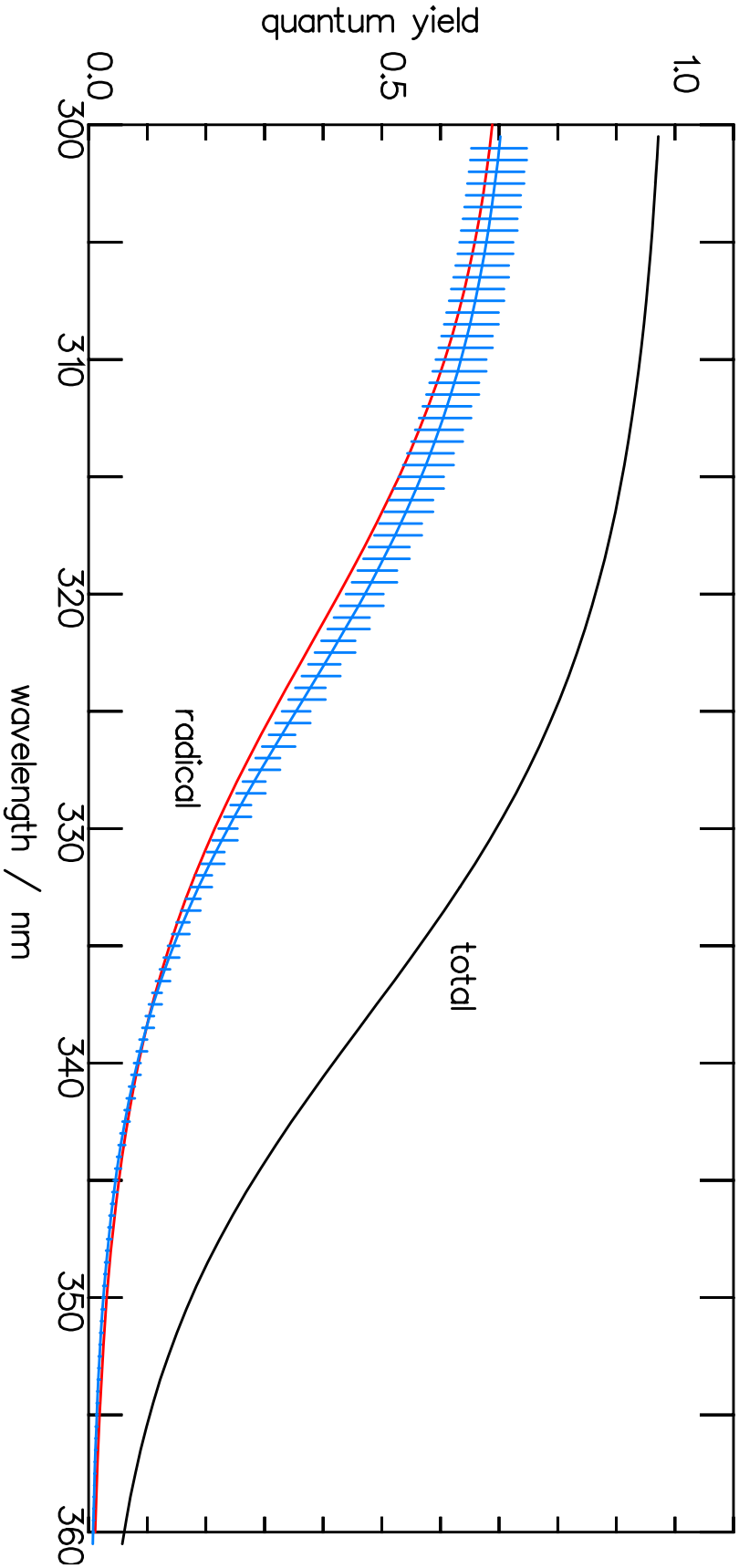
quantum yield
0.0
0.5
1.0
300
310
320
330
340
350
360
wavelength / nm
radical
total

Fig. 10

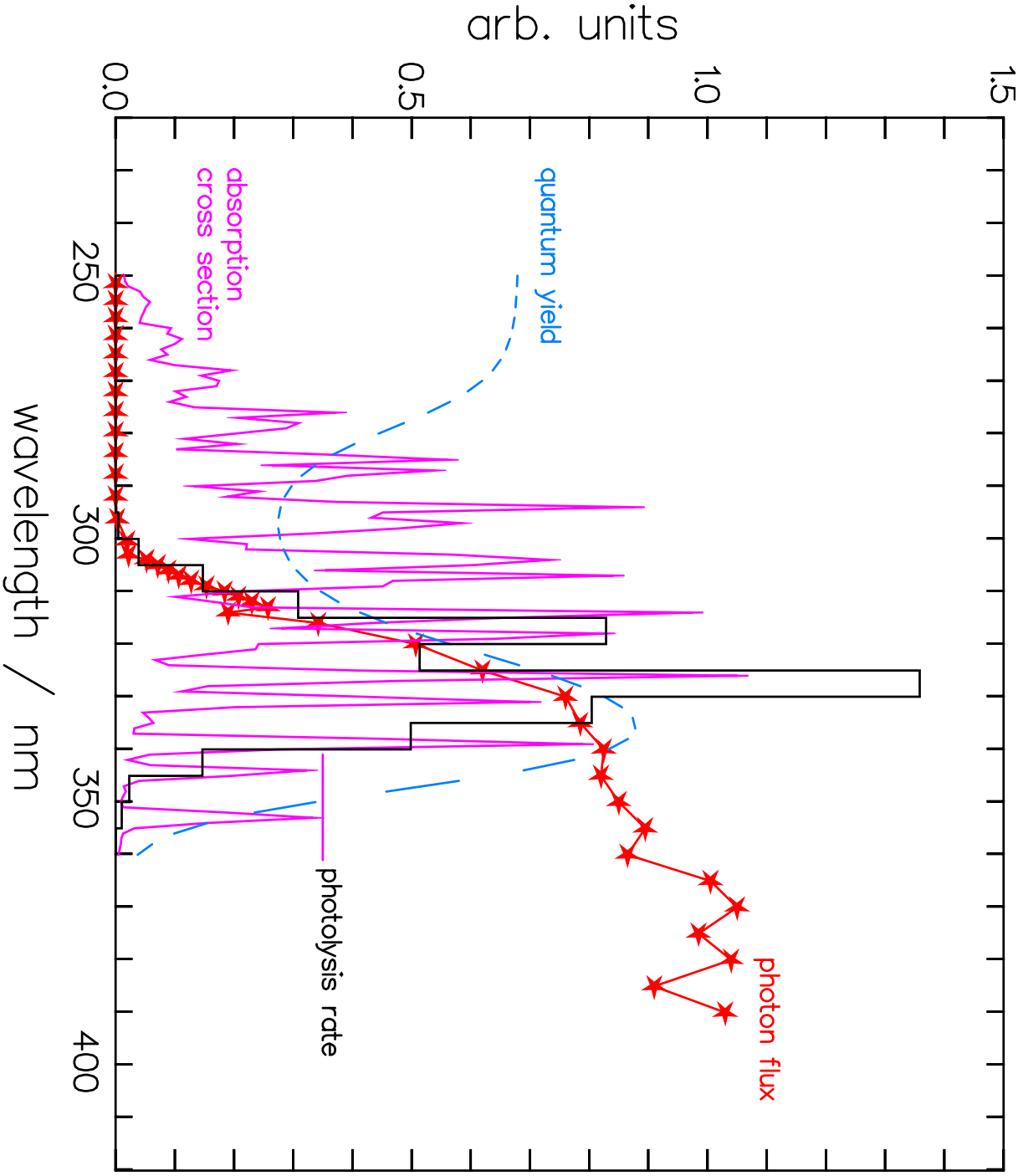
arb. units
0.0
0.5
1.0
1.5
wavelength / nm
250
300
350
400
absorption cross section
quantum yield
photolysis rate
photon flux

Fig. 11

691

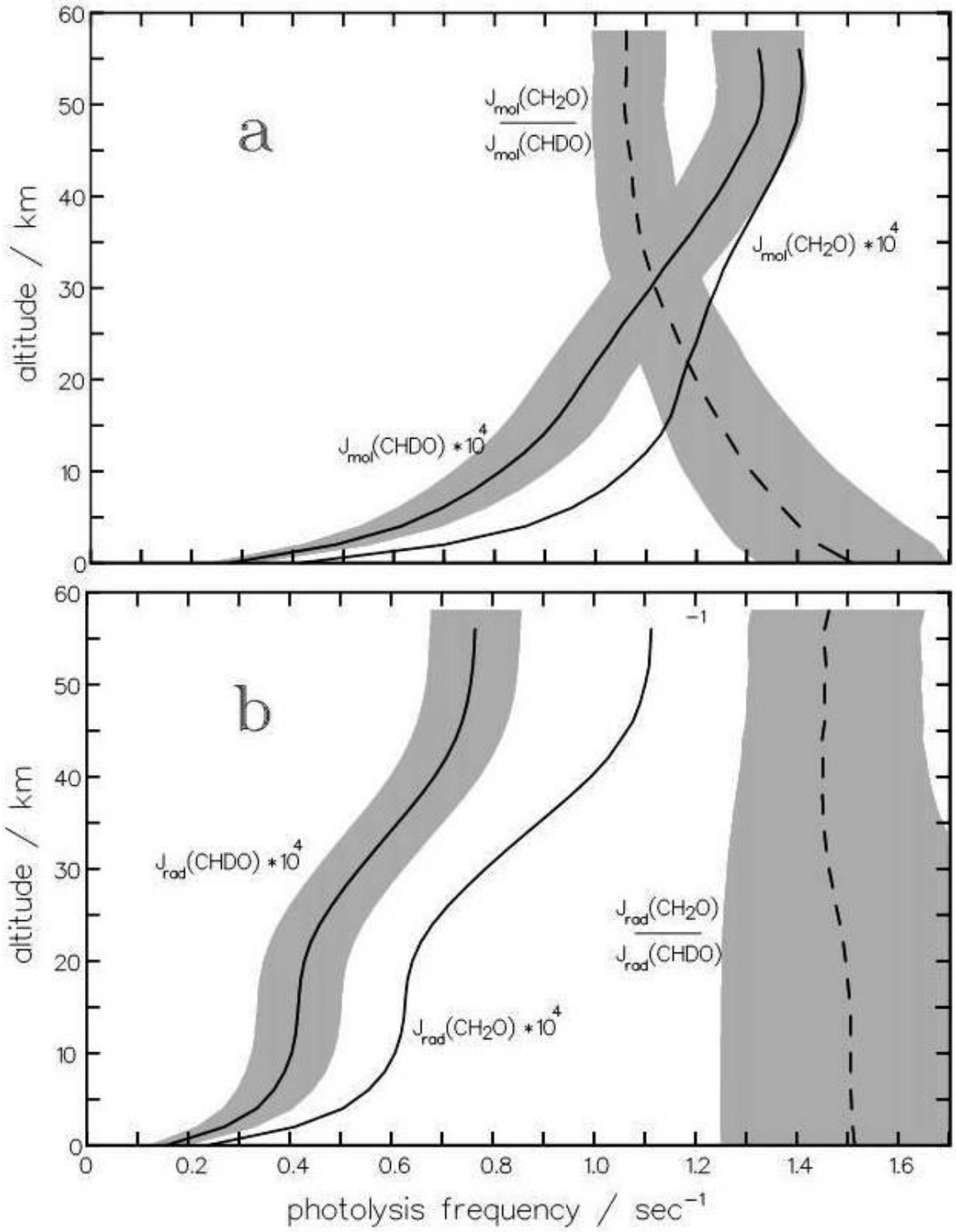

692

693

694

695 Fig. 12

696

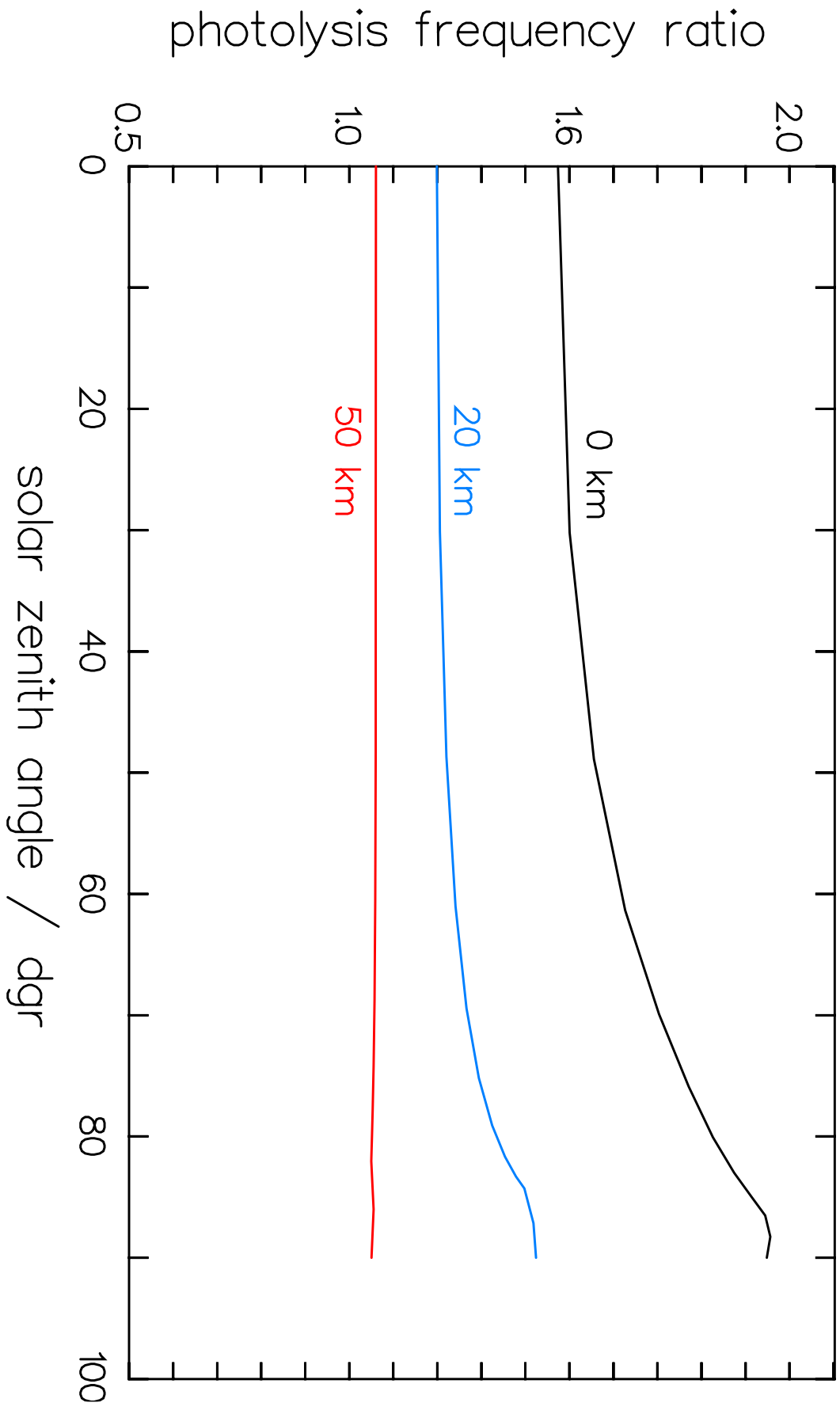
photolysis frequency ratio
0.5
1.0
1.6
2.0
0
20
40
60
80
100
solar zenith angle / dgr
50 km
20 km
0 km

Fig. 13

700

$$CHDO(S_0) + h\upsilon \rightarrow CHDO^*(S_1) \quad \text{(R0)}$$

$$CHDO^*(S_1) \rightarrow CHDO^{\#} + h\nu_1 \quad \text{(R1)}$$

$$CHDO^*(S_1) \rightarrow CHDO^*(S_0) \quad \text{(R2)}$$

$$CHDO^*(S_0) \rightarrow H+CDO \,/\, D+CHO \quad \text{(R2a)}$$

$$CHDO^*(S_0) \rightarrow CO + HD \quad \text{(R2b)}$$

$$CHDO^*(S_0) + M \rightarrow CHDO^{\#}(S_0) + M \quad \text{(R2c)}$$

$$CHDO^*(S_1) + M \rightarrow CHDO^{*\text{-}\Delta\varepsilon 1}(S_0) + M \quad \text{(R3)}$$

$$CHDO^{*\text{-}\Delta\varepsilon 1}(S_0) \rightarrow H+CDO \,/\, D+CHO \quad \text{(R3a)}$$

$$CHDO^{*\text{-}\Delta\varepsilon 1}(S_0) \rightarrow CO + HD \quad \text{(R3b)}$$

$$CHDO^{*\text{-}\Delta\varepsilon 1}(S_0) + M \rightarrow CHDO^{\#}(S_0) + M \quad \text{(R3c)}$$

$$CHDO^*(S_1) + M \rightarrow CHDO^{*\text{-}\Delta\varepsilon 2}(S_1) + M \quad \text{(R4)}$$

$$CHDO^{*\text{-}\Delta\varepsilon 2}(S_1) \rightarrow CHDO^{\#}(S_0) + h\nu_5 \quad \text{(R5)}$$

$$CHDO^{*\text{-}\Delta\varepsilon 2}(S_1) \rightarrow CHDO^{*\text{-}\Delta\varepsilon 2}(S_0) \quad \text{(R6)}$$

$$CHDO^{*\text{-}\Delta\varepsilon 2}(S_0) \rightarrow H+CDO \,/\, D+CHO \quad \text{(R6a)}$$

$$CHDO^{*\text{-}\Delta\varepsilon 2}(S_0) \rightarrow CO + HD \quad \text{(R6b)}$$

$$CHDO^{*\text{-}\Delta\varepsilon 2}(S_0) + M \rightarrow CHDO^{\#}(S_0) + M \quad \text{(R6c)}$$

$$CHDO^{*\text{-}\Delta\varepsilon 2}(S_1) + M \rightarrow \ldots \quad \text{(R7)}$$

701

702

703 Reaction scheme (Table 1)